IEEE Access
Multidisciplinary ⋮ Rapid Review ⋮ Open Access Journal

Received September 26, 2020, accepted October 15, 2020, date of publication October 19, 2020,
date of current version November 11, 2020.

Digital Object Identifier 10.1109/ACCESS.2020.3032161

Oil Plume Mapping: Adaptive Tracking and Adaptive Sampling From an Autonomous Underwater Vehicle

JIMIN HWANG[1], NEIL BOSE[2], HUNG DUC NGUYEN[1], (Member, IEEE), AND GUY WILLIAMS[3]
[1]Australian Maritime College, University of Tasmania, Launceston, TAS 7248, Australia
[2]Office of the VP (Research), Memorial University, St. John's, NL A1C 5S7, Canada
[3]Autonomous Maritime Systems Laboratory, University of Tasmania, Hobart, TAS 7004, Australia

Corresponding author: Jimin Hwang (jimin.hwang@utas.edu.au)

This work was supported in part by the Fisheries and Oceans Canada through the Multi-Partner Research Initiative (MPRI) 1.03: Oil Spill Reconnaissance and Delineation through Robotic Autonomous Underwater Vehicle Technology in Open and Iced Waters, and in part by the Australian Research Council's Special Research Initiative through the Antarctic Gateway Partnership under Project SR140300001. The work of Jimin Hwang was supported by the Australian Government Research Training Program Scholarship.

ABSTRACT We have developed an adaptive sampling algorithm for an Explorer autonomous underwater vehicle (AUV) to conduct in-situ analysis of acoustic measurements to perform autonomous oil plume detection and tracking. The methodology of the tracking phase involves ongoing analysis of the detected plume, assessing target validity and proximity for AUV decision-making for plume mapping. We previously introduced the *bumblebee flight path,* a new biomimetic search pattern designed to maximize the spatial coverage in the oil plume detection phase. This paper focuses on a new tracking strategy as the key adaptive stage in our plume delineation. For initial development we used a 360-degree scanning sonar sensor model. Simulations were done with different plume models to assess the performance of the developed adaptive sampling algorithm. A convergence study demonstrated that the algorithm could successfully track the boundary of a non-regular shaped/patchy oil plume at up to a 0.05Hz sampling frequency. A sensitivity study identified the correlations between plume feature complexity and the anticipated range of acoustic measurement update delays. The decision-making architecture consists of three separate components which implements either proximity or boundary following control and contributes to the final decision on the next desired heading of the vehicle. A weight ratio, that determined the relative allocation of each component, was varied to study its impact on the tracking performance of the AUV. The novelty of our approach is in addressing the discontinuous and patchy nature of realistic oil plumes. Our sampling algorithm and its performance in simulations is a significant step beyond the practical limitations of existing gradient-following methods because it accounts for the oil patches and droplets which gradient-following algorithms do not.

INDEX TERMS Oil pollution, acoustic sensors, sonar detection, unmanned autonomous vehicles, adaptive algorithms.

I. INTRODUCTION

Oil spill accidents are one of the major catastrophes that can occur in the ocean that give rise to irremediable damage to marine wildlife and the marine ecosystem. The effects of a large oil spill are myriad: coastal contamination, loss of aquatic flora and fauna, impacts on human health including death, atmospheric pollution and socio-economic losses for coastal industries. Continuously increasing oil transportation has led many coastal communities to be at risk of oil spill disasters [1]. While surface oil slicks can be detected and mapped by satellite imagery, subsurface oil plumes are more difficult to track, requiring the use of chemical oceanography sensing techniques such as the fluorometric measurement of polyaromatic, refined and crude hydrocarbons [2].

Detection of a sub-surface oil plume is not as straightforward as it may be on the surface. Firstly, subsurface oil plumes are usually transferred by ambient currents from the

The associate editor coordinating the review of this manuscript and approving it for publication was Edith C.-H. Ngai.

origin of the spill. The mixing energy by surface waves accelerate the physical degradation of the hydrocarbon compounds [3]. Also, oil in water often forms a discontinuous plume composed of countless undissolved droplets due to the coalescent and clustering characteristics of oil [4], [5]. It is desirable that there is minimal to zero disturbance of an oil plume by the detection methodology prior to its clean-up. This promotes the use of a non-contact remote sensing approach, as opposed to active interaction within the plume.

To date, most plume-tracking strategies in adaptive mission planning adopt gradient-following techniques [6], [7]. Their targets are usually continuous plumes which have a series of continuous iso-density contours throughout their structure. Gradient-following methods utilise one or more sensors to measure oil concentration at a given point in time. Following the same concentration contour of interest is one approach; discriminating the observation field based on binary sensing (either positive for presence or negative for absence) is another. However, when the subject of interest is oil mixed into seawater, the merits of such approaches are curtailed by the cloud-based nature of the micro-sized droplets in the plume. More recently, huge efforts have been put in artificial learning for adaptive control of robots [8]–[10].

The principal objective of our project is to establish an adaptive sampling system for an autonomous underwater vehicle (AUV) that can swiftly delineate subsurface oil plumes. The essence of an adaptive mission is in optimising the response of a platform to target parameters that are unknown prior to deployment, such as where the target is or where the target is headed. This can be achieved by utilising in-situ data that is analysed in real-time with an additional onboard computer called a Backseat Driver that is able to send instructions to modify the mission of the platform. The result is a higher intelligence approach that extends the autonomous capabilities of an AUV platform.

Here we have developed an adaptive sampling system for the Memorial University of Newfoundland (MUN) Explorer AUV [11] to autonomously delineate an oil plume. The algorithm successfully simulated the following tasks: oil plume tracking, boundary mapping of a patchy plume and the triggering of a water sampler. Determining our plume tracking strategy demanded a full scan around the AUV, we extended our sensor model from a 90-degree-forward-looking survey to a 360-degree survey. We additionally generated different oil plume shapes to evaluate the robustness of our tracking algorithm. In this paper, we describe our designed adaptive mission planning algorithm. In Section II, we summarise our decision-making strategy for plume tracking and water sampling. The AUV mathematical model, the sonar sensor model, and the plume models that we generated for simulation are illustrated. The simulation results are described and analysed in Section III. As part of this analysis, we evaluate the minimum required sampling frequency through a convergence study; then a sensitivity study is presented so as to investigate the influence of each parameter on tracking behaviour. In Section IV, we present an enriched analysis to emphasise the combined effect of multiple parameters.

II. METHODOLOGY

A. DESCRIPTION OF ADAPTIVE MISSION DESIGN

The developed adaptive sampling procedure includes two phases: A *Searching* phase and a *Tracking* phase. Each phase consists of two iterative modes and each mode is automatically triggered when certain conditions are met (Figure 1.) We previously presented the *Initialisation, Searching* and *Detection* phases [11]. This paper primarily focuses on our new tracking strategy during the *Tracking* phase to adaptively track an oil plume without any prior knowledge about the plume or pre-set AUV trajectory.

Once the AUV is deployed, random waypoints are assigned within the designated two-dimensional operational area by the *waypoint-generator* function during Mode 1 (*Waypoint-visiting mode*). Then the *trajectory-planner* function generates an optimum path based on a genetic solution for the Traveling Salesperson Problem [12]. Mode 2 (*Bumblebee-flight-search mode*), is triggered to expand the search area around each waypoint by following a bumblebee flight path. Sensor signals are continuously observed during both modes to seek any sign of the oil plume, alternating between Mode 1 and Mode 2 until oil detection is made and confirmed. Further details of the *Searching* and *Detection* phase can be found in [11].

Once it is suspected that an oil plume is present, Mode 3 (*Plume-tracking mode*), is triggered and the vehicle starts to autonomously track the plume. The vehicle's next heading angle and location are determined based on the sensor data. The aim of Mode 3 is to follow the boundary of the plume, maintaining an offset distance, and mapping it in real time. When mapping is complete and the AUV returns to the location at which Mode 3 began, Mode 4 (*Water-sampling*) starts.

This sampling procedure is conducted in a relatively less disruptive way by having the vehicle follow a single pass through the plume as opposed to movements involved with making multiple turns. The decision-making mechanism involved in each mode and the calculation algorithm are described in the following sections.

B. PING360 SCANNING SONAR MODEL

Contactless detection of a subject in the environment around an AUV can be performed by optical or acoustical methods or a combination of both [13]. Optical data can be acquired from a visual sensor such as an underwater high-resolution still or video camera [14] or a laser system [15]. While the use of visual detection is intuitive, optical images require a great deal of processing time to analyse. Given present levels of onboard computing capacity, it is currently impractical to execute an adaptive mission that relies on optical image analysis in real time. While sonar data tends to be noisier

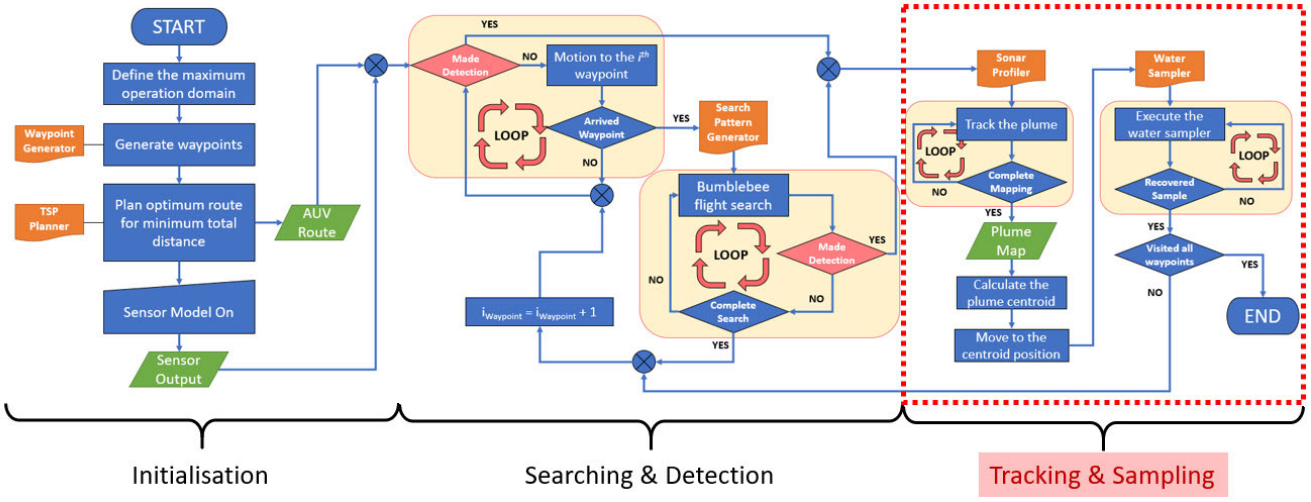

FIGURE 1. Flowchart describing the designed adaptive sampling procedure. Tracking and Sampling phases, with two independent iteration blocks, are highlighted.

compared with camera images [16], they do not need the high-intensity discharge lights required by optical sensors in deep water operations. Sonar-based sensors are robust units that have been widely used for underwater navigation [17], bathymetry [18] as well as obstacle detection [19].

A meso-scale test was first conducted to prove the concept of using sonar to detect an oil plume. In the test a BV5000 sonar (*Teledyne Blueview*), with a relatively high frequency of 1.35MHz, was found to distinctly capture oil plume motion. We then constructed a sensor model with 360 degrees of azimuth angles relative to the AUV and a 50m range. Our sonar sensor model was built based on the *Ping360* scanning imaging sonar that is being integrated on the Explorer AUV. The default sampling frequency of the *Ping360* is 0.2Hz; which means that it takes 5 seconds to collect a complete set of 360-degree data. Each cell is modelled to have 16-bits of data which represent the sonar echo strength. Hence the model discretises the acoustic intensity between 0 and 65,535.

Outputs from the model included the instantaneous AUV location, the current AUV heading angle and an array of the sonar intensity measurements. The sensed plume is displayed in two frames of reference: the global view (A and C) and the AUV view (B and D) as shown in Figure 2. The former was used for the mapping task while the latter determines the required change of AUV heading angle in the decision-making step.

C. AUV MATHEMATICAL MODEL

The AUV position on the plane was specified in the global frame of reference (GFR) as well as the local frame of reference (LFR). We used the basic kinematic model of the AUV that was previously developed [11].

The inverse transformation matrix was used to transform the AUV motion along the axes of the GFR to the LFR.

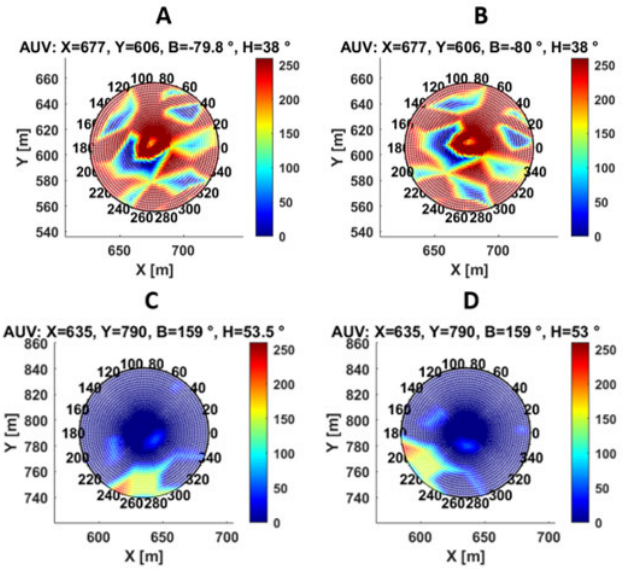

FIGURE 2. Example outputs from the scanning sensor model at the AUV position: X, Y coordinates (677, 606) and (635,790) respectively. The sonar screen is shown in the global frame of reference (A and C) and in the AUV frame of reference (B and D).

Equation (1)-(3) show the multiplication process using the transformation matrix.

$$\xi_{position} = \begin{bmatrix} x \\ y \\ \theta \end{bmatrix} \xi_{velocity} = \begin{bmatrix} \dot{x} \\ \dot{y} \\ \dot{\theta} \end{bmatrix} \xi_{acceleration} = \begin{bmatrix} \ddot{x} \\ \ddot{y} \\ \ddot{\theta} \end{bmatrix} \quad (1)$$

$$R(\theta)^{-1} = \begin{bmatrix} \cos\theta & \sin\theta & 0 \\ -\sin\theta & \cos\theta & 0 \\ 0 & 0 & 1 \end{bmatrix} \quad (2)$$

$$\xi_{global} = R(\theta)^{-1}\xi_{AUV} \quad (3)$$

The coordinates in both frames of reference are interchangeable [20]. The AUV pose (x, y, θ) in the GFR was used

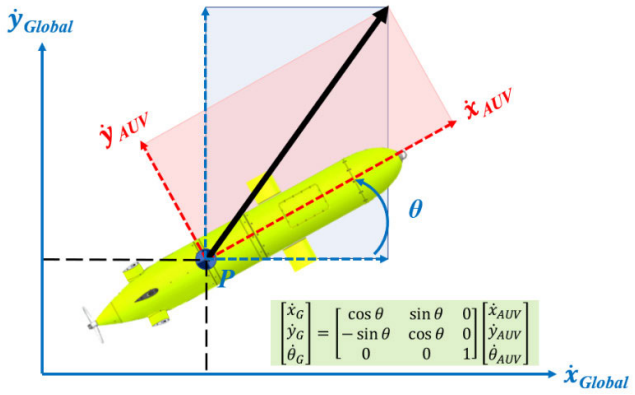

FIGURE 3. AUV velocity components in the global and local frames of reference.

during plume mapping, while those in the LFR were used during the decision-making process. The velocity components of the AUV in the global and the local frame of reference are illustrated in Figure 3.

D. IN-SITU DATA ANALYSIS

The tracking algorithm consists of a recursive *Measure-Analyse-Action* iteration process. The ultimate outcome of the iteration is the next target heading angle of the vehicle.

Firstly, in the *Measure* stage, the sensor model continuously takes data from the sonar. This data contains a set of information including the relative position of the measurement to the AUV in polar coordinates (*range* and *azimuth angle*) and its echo strength (*intensity*). The total sum of the intensities, *Aggregate*, is calculated using the sum equations (4)-(5). *Aggregate* indicates whether the vehicle has come close to an oil plume by comparing its value with $Threshold_{ENTRÉE}$. The maximum intensity value that one grid cell can contain is 65.5×10^3. As there are 50 grid cells per 1 degree, the maximum value of *Aggregate* is approximately 11.8×10^8 for the full 360-degree data set.

$$measurement = \begin{bmatrix} range & azimuth & intensity \end{bmatrix} \quad (4)$$

$$Aggregate = \sum_{k=1}^{360} measurement(k, 3) \quad (5)$$

In the *Analysis* stage, the analysis function examines the measured data. The obtained data is initially subject to a *Total-sum test* and a *Sector-sum test* as illustrated in Figure 4. The *Aggregate* value indicates the overall proximity of the vehicle to the plume by comparing it with pre-set threshold values. Table 1. lists the four thresholds that are set for the detection state. These values are used to identify the desired AUV status in relation to the plume. In the *Total-sum test*, therefore, *Aggregate* and the *Thresholds* were compared to determine the AUV status in terms of plume detection as shown in equations (6)-(8). $Threshold_{ENTRE}$ and $Threshold_{EXIT}$ are entry and exit levels that indicate whether the strength of the sonar signal is sufficiently strong or weak

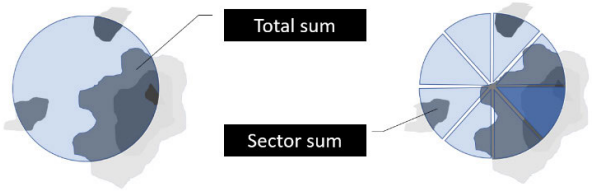

FIGURE 4. Total data sum (left) and sector sums (right) of the sonar window.

TABLE 1. Descriptions of thresholds set for detection state.

Threshold	Value	AUV Status
$Threshold_{ENTRE}$	25.72E6	Detection is made
$Threshold_{EXIT}$	2.57E5	AUV has lost the plume
$Threshold_{MAX}$	707.78E6	Too close to the plume
$Threshold_{MIN}$	235.93E6	Too far from the plume

enough to presume that the plume is inside the sensing environment of the AUV. $Threshold_{MIN}$ and $Threshold_{MAX}$ indicate the minimum and maximum allowable level of *Aggregate* for threshold control analogous to a thermostat controller. The values must be given in ascending order from $Threshold_{EXIT}$, $Threshold_{ENTRE}$, $Threshold_{MIN}$, and then to $Threshold_{MAX}$. The values of these thresholds were carefully selected as these values influenced the performance of the proposed process. We recommend that new users try our adjusted values; then tune them for a given application. These values are subject to change with respect to the desired AUV proximity to the plume as determined by the mission details.

$$Boolean.Aggregate \geq Threshold_{ENTRE} \quad (6)$$

$$Boolean.Aggregate \leq Threshold_{EXIT} \quad (7)$$

$$Threshold_{MIN} \leq Aggregate \leq Threshold_{MAX} \quad (8)$$

Subsequently, the *Sector-sum test* splits the sonar window into eight sectors. Then, it provides vector results which include eight sets of desired direction and magnitude. Their vectorized sum, combined with the $p_{coefficient}$ from the first test, finally provides the value of *proximity angle*, which is the heading angle that ensures the vehicle stays between $Threshold_{MAX}$ and $Threshold_{MIN}$ (See Figure 5.). However, it is not used independently, but in combination with the *edge angle* and *adjustment angle* to obtain the *resultant angle* as described in the next sections.

E. DECISION-MAKING ARCHITECTURE OF TRACKING

In the *Action* stage, the information including the resultant heading angle is calculated and then finally sent to the vehicle control system. The decision on the resultant heading angle combines three factors: *edge angle*, *proximity angle* and *adjustment angle*. They are listed with a description of their roles, respectively in Table 2.

The *proximity angle* is calculated using the outcomes (p_{factor} and $p_{coefficient}$) from both tests (*Total-sum test* and

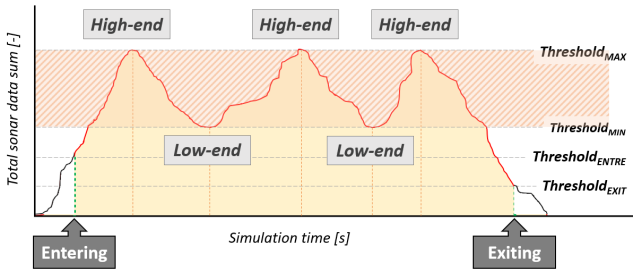

FIGURE 5. An Aggregate plot during Mode 3 simulation. Keeping the vehicle at a fixed distance from the plume was done using this thresholding control.

TABLE 2. The role of each coefficient of each angle term.

Angle	Factor	Relevant test	Role/ Control
proximity	p_{factor} $P_{coefficient}$	Total sum Sector sum	Proximity
edge	*edge angles*	Patch-identification Plume-ahead Edge-line angle	Left-side plume edge following
adjustment	*offset*	Gradient test	Damping effect

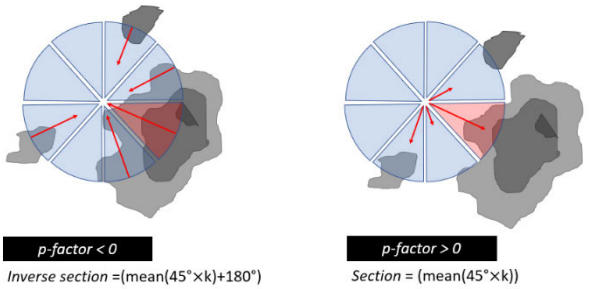

FIGURE 6. Outcomes of calculating $sector_k$ defined by p_{factor}. Inverse section is used in the negative p_{factor} case (left) and section is used in the positive p_{factor} case (right).

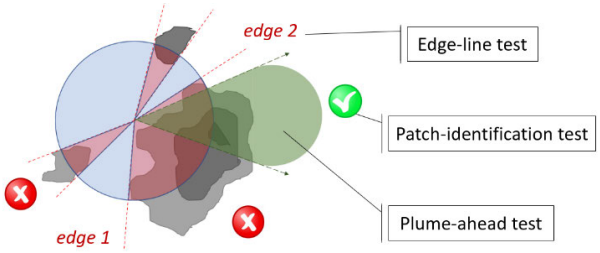

FIGURE 7. Three tests involved in the edge angle term calculation including Plume-ahead test, Patch-identification test and Edge-line test.

Sector-sum test). Its primary role is proximity control which keeps the vehicle at a desired distance from the plume so that the plume is not lost during operation nor unnecessarily disturbed. While p_{factor} represents the sign (either positive or negative), $p_{coefficient}$ defines the proximity quantity (how close the vehicle gets to the plume). These outcomes determine whether to move closer or further away from the plume. For example, a positive p_{factor} means low proximity. Hence, the vehicle needs to get closer to the plume. On the other hand, a negative p_{factor} means high proximity, which indicates that the vehicle is at a closer distance than desired. The *proximity angle* is found from equation (9)-(12) as below.

$$proximity = \arctan\left\{p_{coefficient}(y), p_{coefficient}(x)\right\} \tag{9}$$

where $p_{coefficient}$ is found by resolution from:

$$\begin{aligned} p_{coefficient}(x) &= \sum_{1}^{k} \cos\left(\sec tor_k\right) \times proportion_k \\ p_{coefficient}(y) &= \sum_{1}^{k} \sin\left(sector_k\right) \times proportion_k \end{aligned} \tag{10}$$

where the $sector_k$ determines the direction of each sector (see Figure 6.), depending on the sign of p_{factor}.; and the $proportion_k$ is the ratio of S_k (the sum of the sonar readings in each sector) to the $sector_{MAX}$ (the possible maximum value of S_k).

$$sector_k = \begin{cases} mean(45^\circ \times k), & p_{factor} = -1 \\ mean(45^\circ \times k) + 180, & p_{factor} = +1 \end{cases} \tag{11}$$

$$proportion_k = (s_k / sector_{\max}) \tag{12}$$

The *edge angle* is the primary angle term to enforce the vehicle to follow the plume boundary while maintaining the plume on the right-hand side of the vehicle. The vehicle could follow the plume by either keeping the plume on the left- or right-hand side of the vehicle. In this work the plume was always maintained on the right side of the vehicle so as to avoid confusion with the direction of the vehicle. To calculate the target *edge angle*, a set of sequential tests must be done first including a *Patch-identification test*, a *Plume-ahead test*, and an *Edge-line test*. Firstly, in the *Patch-identification test*, each scan line (1° – 360°) is subject to inspection to identify whether oil droplets lie on the scan line. Discrimination among detected lines and non-detected lines indicates the separation of each patch (discontinuity). So, the total number of patches are identified in the first test. Subsequently, the *Plume-ahead test* analyses whether the detected patches lie within a 40-degree swath ahead of the vehicle (See Figure 7.). This is the azimuth 20 degrees either side of the vehicle's zero-degree heading. If there is a patch lying ahead, any other patches are excluded in the rest of the analysis. If there are no patches detected ahead, the patch of the highest interest is selected for consideration. The highest interest in this context is defined by the relative direction of each identified patch to the AUV heading and the patch density.

The sonar can encounter various 'complete' patch boundaries for oil plumes with different shapes and density or just 'partial' ones (See Figure 8.). Cases A to D are the basic examples where an oil plume lies ahead of the vehicle. For example in Case-A, a partial patch behind a complete but small sized island is selected to be of interest for identification, while in Case-B, the two light islands (less than a certain level of oil density) are ignored and the vehicle is directed to pass through or between them. Similarly, a partial light peninsula is ignored in Case-C; however, an *edge angle* is

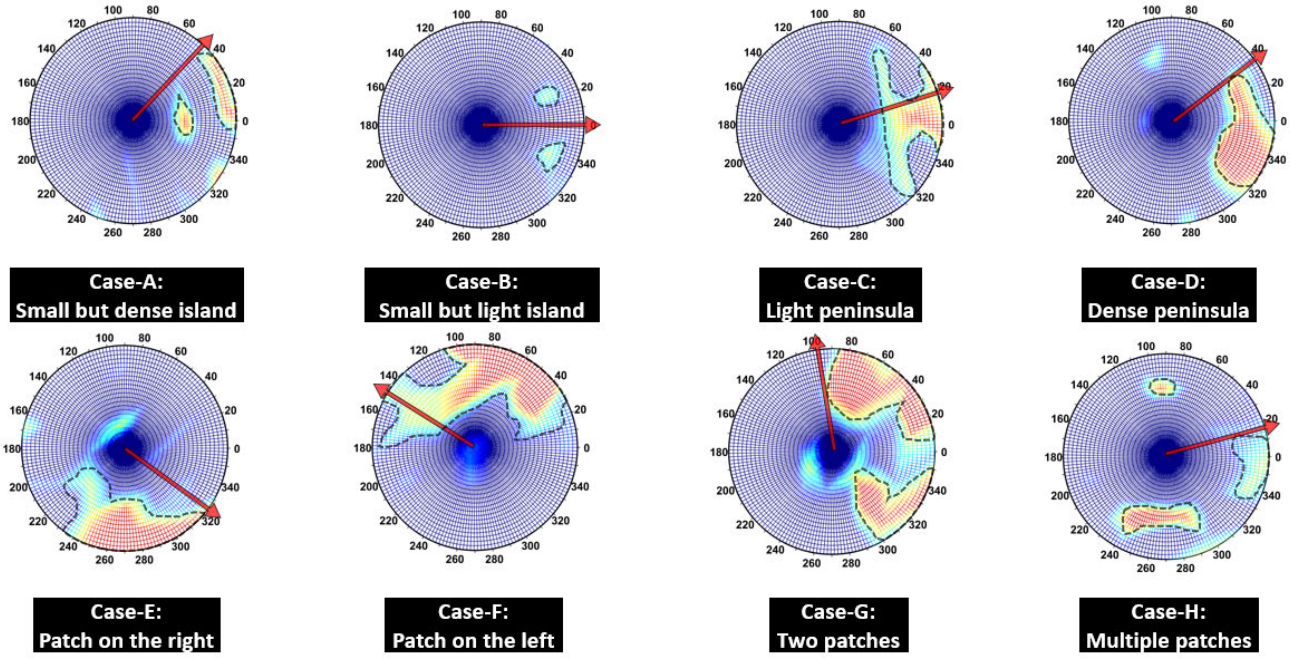

FIGURE 8. Various patch boundaries that the sonar may encounter: the patch of the highest interest is selected depending on its position and its density. The edge-angle is determined after the Plume-ahead and Edge-line test, as marked by the red arrow. A heading of 0 degrees is the heading of the vehicle.

selected as the direction where the vehicle can pass to the left side of the plume in Case-D. The same is true in Case-E and F where the plume does not lie ahead. When multiple patches are detected like in Case-G or H, either the stronger density patch is selected, or the patch ahead is selected if there is a gap that the vehicle can pass through. Finally, a required turning angle (*edge-angle*) is estimated through an *edge-line test.*

The *adjustment angle* was introduced to prevent the vehicle from being stuck at a sudden bulging edge of the plume (which was found to occur in early simulations). The *adjustment angle* is a function of the *offset* and aims to prevent sharp turns in heading. A linear interpolation formula was used to calculate the *adjustment angle* as shown in (13).

$$adjustment\ angle = 2\varphi\,(s_t - s_{t-1} - g_{\min}) \,/\, (g_{\max} - g_{\min}) \tag{13}$$

where

$s_t - s_{t-1} =$ *gradient of Aggregate,*
$g_{min} =$ *minimum gradient,*
$g_{max} =$ *maximum gradient,*
$2\varphi =$ *the offset angle range,*
$\psi =$ *the gradient proportion factor*

Values of g_{min} and g_{max} is found from:

$$g_{\min,\max} = \pm\psi \times Aggregate_{MAX} \tag{14}$$

Through empirical simulations, effective values of φ and ψ were found to be 5.0 and $\pm 2.5\%$ of the $Aggregate_{MAX}$, respectively. If the gradient is zero (no change in the total signal sum), the *adjustment angle* is set to the default value of *offset*. The *offset* is an input set by the operator, somewhere in the range from 10 to 40. A discussion on the choice of this angle is given in Section IV. The pseudo code of the decision-making process for the resultant angle is given in Figure 9.

There are two ways in which it was assumed that the vehicle could extract itself from being stuck in this type of situation. Firstly, when the detection is no longer valid, i.e. that the vehicle has lost contact with the plume, the tracking is terminated, and the AUV reverts back to the searching mode. Secondly, when the vehicle returns to the location at which the tracking started, the tracking is considered complete and the mission moves on to the next sampling mode. The various coefficients described above were tuned via a sensitivity study, which is described in the results section. The process to calculate the final resultant heading angle is presented (See Figure 10.).

F. VIRTUAL HYDROCARBON PLUME MODELS

Virtual hydrocarbon plume models were designed to emulate as realistic an oil plume as possible in the simulation domain. The models represented static two-dimensional discrete oil plumes with diverse shapes and random patterns. They consisted of mixed patches of micro-sized oil droplets. They were created based on the results obtained from two preceding oil sensor experiments. The first test was done in the wave tank at the Bedford Institute Oceanography (BIO) and the second in Port au Port Bay [4]. During the first experiment, oil in water was observed to form a number of patches and clouds

```
if mode == plume-tracking
while true
%% MEASURE Stage:
[sonar]= collect[sensor_measurement]
%% ANALYSIS Stage:
% Total-sum test
if Total_sum <threshold_exit; break
[sector]=[sector1 ~ sector8]
% Sector-sum test
if Total_sum > threshold_max; p_factor = -1
elseif Total_sum < threshold_min; p_factor = +1
else interpolate p_coef
%% DECISION-MAKING Stage:
% Edge_angle calculation:
% Patch test(1): Patch identification
find number_of_patches; patch(n)={p1,p2,p3...pn}
% Patch test(2): Plume_ahead test
if plume_ahead_exist; select the patch ahead
else distribute weight for each patch;
    select the patch with the highest weight
% Patch test(3): edge_test
examine k=[360/1]{scan_line_k};
find edge_angle_1 && edge_angle_2
edge_angle = edge_angle_2
% Proximity_angle calculation:
vectorised_sum(sector[i=1:8])
if p_factor > 0;
  proximity_angle = p_coef*highest_sector
elseif p_factor < 0;
  proximity_angle = p_coef*lowest_sector
% Adjustment_angle calculation:
gradient = previous_sum - current_sum
adjustment_angle = interpolate g_coef;
Resultant_angle =
f{edge_angle, proximity_angle, adjustment_angle}
```

FIGURE 9. The pseudo code for calculating the resultant heading angle including the three terms (edge angle, proximity angle and adjustment angle) through a sequential set of calculations.

of droplets of various sizes and hence oil concentrations. The outcomes indicated that our AUV control algorithm should account for the discontinuous form of a real oil plume.

Six different plume models with varied density distribution, different levels of roughness of the boundary, patchiness and with a varied number of holes inside the plume were generated as shown in Figure 11. They were labelled from A to F. The reference number as given in (15) roughly indicates the tendency of the plume shape and patchiness. For example, a higher value of the term *incohesion* corresponds to a relatively incohesive plume with a greater number of small holes and patches; whereas a lower value results in a cohesive plume consisting of a continuous body with a smaller number of holes. The *Angularity* term indicates the tendency to have more right-angled or sharp-angled corners. Therefore, a lower *Angularity* number means a relatively circular shaped plume. In summary, model F with a higher *incohesion* number and *angularity* term is likely to be more challenging for the developed algorithm to robustly control the AUV in encircling the plume.

$$\textit{Plume model Ref .no} : \textit{incohesion} - \textit{angularity} \tag{15}$$

where $20 \leq \textit{incohesion} \leq 40$ and $\textit{angularity} \in \{15,25\}$.

G. WATER SAMPLE TRIGGER

In the final mode, the AUV makes direct contact with the plume in order to take a water sample (or it could be another measurement using a sensor that requires direct contact with the plume). When the AUV has completely encircled the plume and has reached a completed mapping, the algorithm automatically switches on the *centroid estimator* which estimates the approximate centroid of the mapped plume. Points on the AUV trajectory were assumed to be a group of same-mass particles. The location of the centre of mass of these distributed particles was found. The weighted sum of the positions of the particles was calculated. In this application, the weighting factors for all particles were equally distributed with the assumption that only the geometrical plume area was required to be found. The method to calculate the centroid of the plume is given in (16).

$$\bar{x} = \sum_{k=1}^{n} \frac{m_k x_k}{\sum_{k=1}^{n} m_k} \quad \bar{y} = \sum_{k=1}^{n} \frac{m_k y_k}{\sum_{k=1}^{n} m_k} \tag{16}$$

where

$n =$ *the number of particles,*
$m_k =$ *the weighed mass of the* k^{th} *particle,*
$(x_k, y_k) =$ *the coordinate of the* k^{th} *particle*

The data flow diagram between the Backseat Driver Computer (Payload Computer) in which our developed adaptive sampling algorithm is implemented and the Frontseat Driver Computer (Vehicle Control Computer) which controls the thruster, planes, water samplers and other equipment is shown in Figure 12. The *Ping360* scanning sonar continuously collects the information from the surroundings. These measurements are processed and analysed; then a decision is made on the new desired heading inside the Backseat driver computer (the speed remains constant). This decision is passed on to the main vehicle control computer which creates commands for the required adjustment of the plane angles and the thruster revolutions.

A triggering signal is sent out to the VCC when the vehicle arrives at the estimated location of the centroid, $(\bar{x}, \bar{y})$. In the field, there is a slight possibility that the calculated position accidently occurs at a hole due to the patchy attribute of a plume. To prevent such a case occurring, a hydrocarbon sensor might be used as a backup to the primary sonar sensor to confirm oil presence at that location. Therefore, the water samplers are triggered only when three requirements are satisfied: arrival of the AUV at the location of the centroid; a positive sonar sensor reading for the presence of oil; and a positive in-situ oil sensor reading such as a fluorometer.

III. SIMULATION RESULTS

The proposed adaptive sampling method was evaluated though simulations targeting different plume models that were generated. A convergence study was done by using varied values of the sampling frequency. The results revealed that a more complex plume model required more prompt

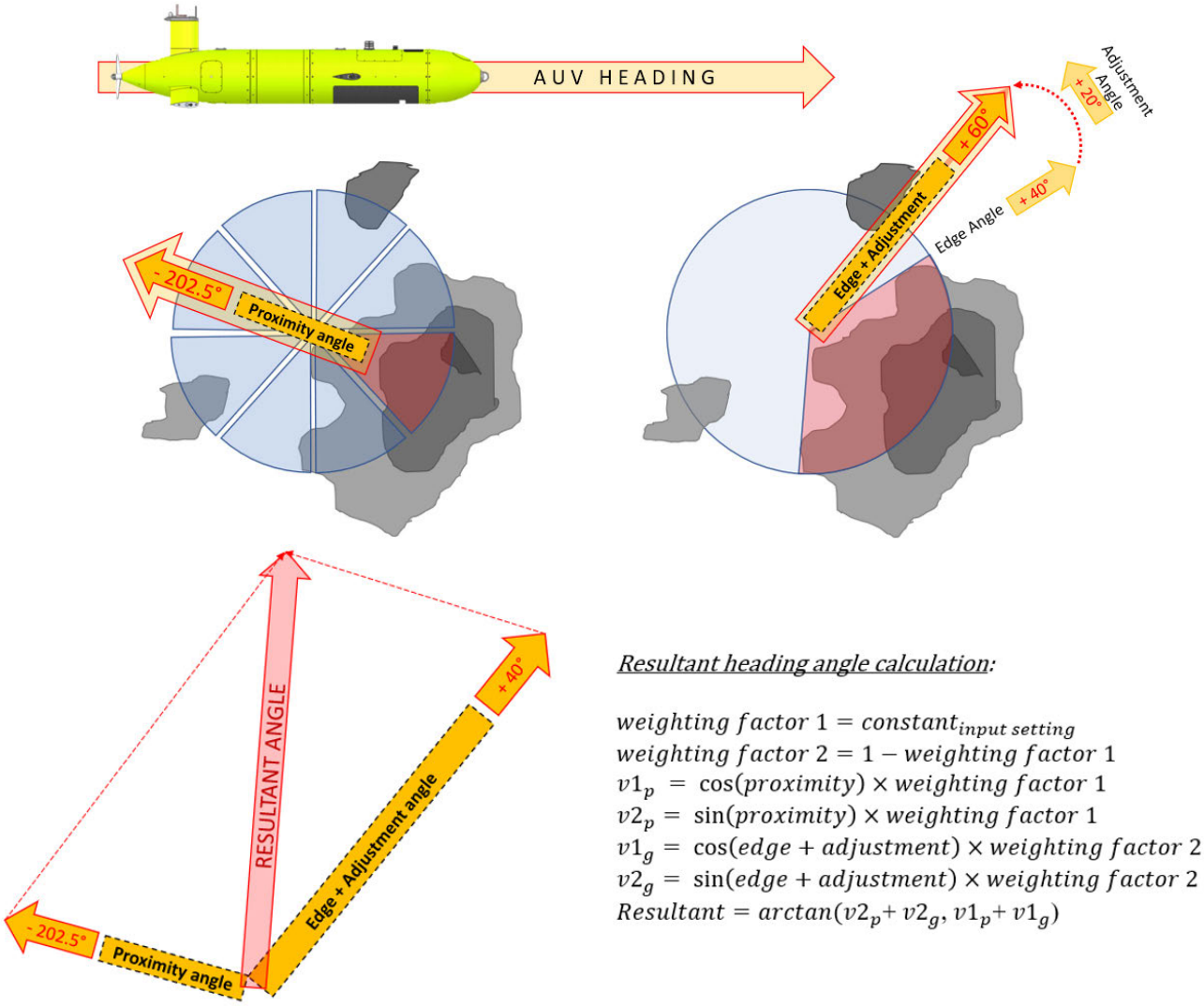

FIGURE 10. The calculating process of the final resultant angle as a function of proximity angle, edge angle and adjustment angle.

adaptation to adjust the heading of the vehicle. A guideline for the maximum time delay allowed for in-situ data processing time between sampling. In addition, a sensitivity study was done with coefficients and thresholds varied. The mapped plumes are presented.

A. CONVERGENCE STUDY

In theory, more frequent sonar measurements are desired to reduce estimation errors [21]. However, a higher number of sensor measurements can lead to excessive computer loads for data processing and hence, delays in real-time analysis and control that exceed the time step between measurements. So, it is crucial to find the operational sampling frequency range balancing the computational load for analysing measurements and the maximum tolerance required to not lose the plume during tracking. Practically, it takes approximately 9 seconds for a complete 360-degree scan using the *Ping360* scanning imaging sonar. Therefore, the algorithm must be sufficiently robust to overcome transmission latency without losing contact with the target plume.

In practice, approximately 72 degrees of sonar dataset will be successively obtained every second. However, in this simulation, we assumed that a full set of data was acquired instantaneously; the errors induced by the actual delay were assumed to be small.

A convergence study was conducted (see Figure 13. And Table 3) to determine the minimum useable sampling frequency, reflecting the allowable time delay that could be tolerated in the real-time Backseat Driver adaptive operation. The useable sampling frequency varied depending on the complexity of the plume model. The minimum useable frequency was found to be 0.33 Hz for models A, B and C (see Figure 14). This tolerance decreased with the complexity of the model, which meant that the minimum useable frequency must be increased for higher incohesion numbers. Models E and F were found to require a minimum frequency

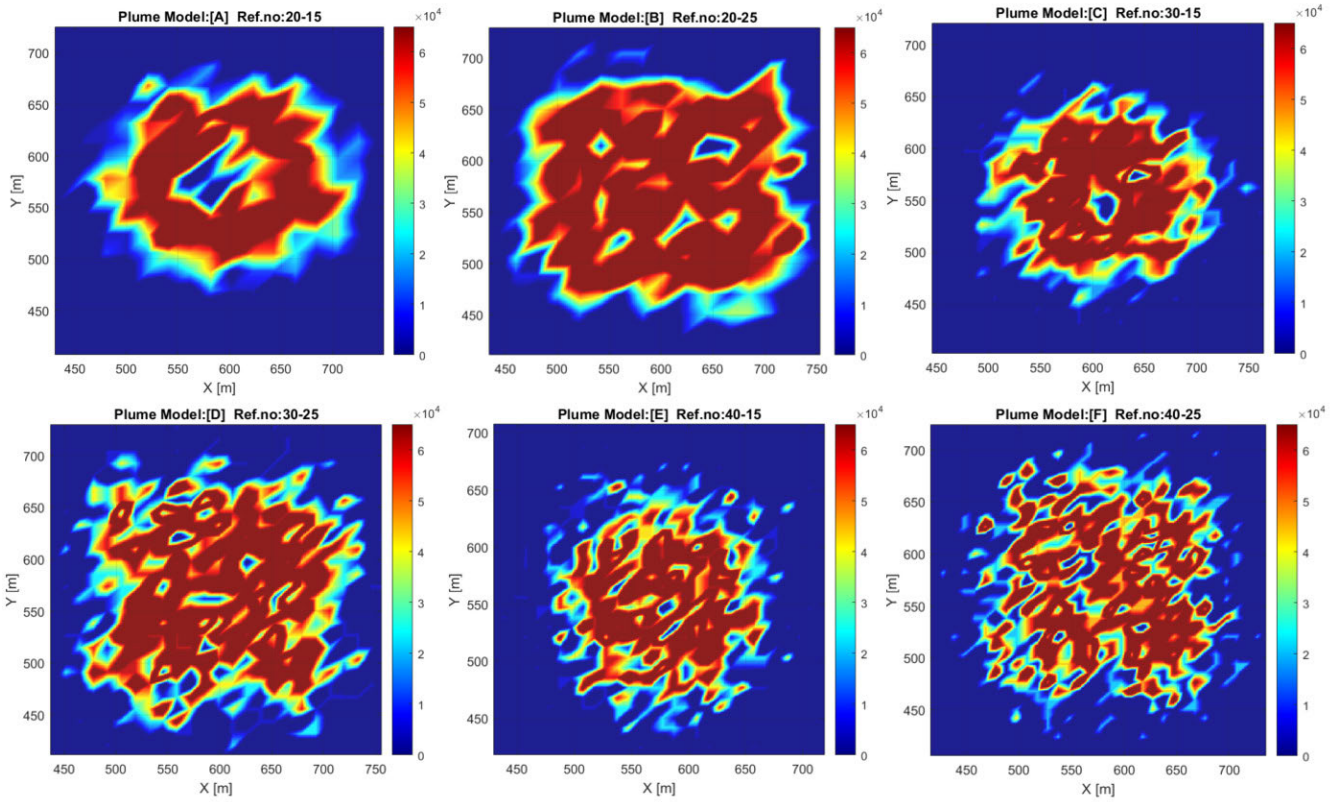

FIGURE 11. Six virtual oil plume models, named A to F. The data set was generated based on acoustic signal strength range (0 ∼ 65,535). Density distribution, levels of roughness of the boundary, patchiness and the number of holes inside the plume is varied between the models.

TABLE 3. The results of the convergence study.

Reference	*incohesion*	*angularity*	Min Frequency
A	20	15	0.033
B	20	25	0.033
C	30	15	0.033
D	30	25	0.040
E	40	15	0.048
F	40	25	0.048

of 0.048Hz. Hence overall, 0.05Hz was found to be the safe minimum useable frequency for all plume models simulated. This means that if the time lag between sonar measurement updates during tracking mode takes longer than around 20 seconds (lower than 0.05Hz frequency), the vehicle is likely to lose contact with the plume it is tracking.

The tracking trajectories for all plume models simulated are shown in Figure 14.

B. SENSITIVITY STUDY

A sensitivity study was conducted for the coefficients that were the key functions in calculating each angle term during the decision-making process. Four terms were tested to evaluate robustness and adaptive capability of the designed algorithm. Model F, the most complicated plume model, was selected for this study to account for the most realistic plume representation. The test was done for the four terms including: *Thresholds*, $p_{coefficient}$, *weighting-factor* and *offset*.

Adjusting the *Thresholds* did not noticeably affect tracking outcomes in terms of the AUV behaviour except for $Threshold_{ENTRE}$. The value of $Threshold_{ENTRE}$ determined the proximity of the AUV to the oil plume at which the first avoiding behaviour was taken. Normally $Threshold_{ENTRE}$ was set between 0.001 – 0.1% of the $Aggregate_{MAX}$ value.

A study was done to determine the influence of p_{factor}. The value of p_{factor} was changed between ± 1 and ± 1000 (logarithmic steps were used). Changing the magnitude of p_{factor} did not influence the overall tracking result.

The *weighting-factor* and *offset* was found to have a significant impact on the tracking behaviour (See Figure 15.). The *weighting-factor* represents the weight ratio of the *proximity angle* term. So, if the *weighting-factor* is 0.3, 30% of weight is allocated to the *proximity angle* term and the rest of the weight (70%) is allocated to the *edge angle* in decision-making on the resultant heading angle (Figure 10.). The range of successful values (that is those values for which tracking of the plume was completed) was between 0.01 and 0.2. The vehicle tracked at a larger distance from the plume at the lower successful values of the *weighting-factor*. Increasing the *weighting-factor* led the vehicle to more closely follow the plume. At a *weighting-factor* of 0.3 the vehicle became stuck

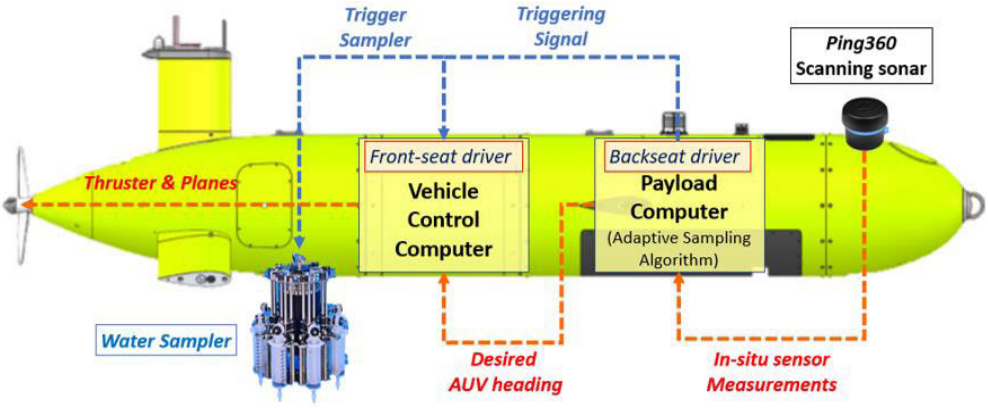

FIGURE 12. Sensor measurement and sampling triggering data flow diagram on board the AUV through the Backseat Driver Computer (Payload Computer) and the Frontseat Driver computer (Vehicle Control Computer). The red dotted line corresponds with the sensor data flow for manoeuvring and plume-mapping. The blue dotted line indicates the water sampling command line.

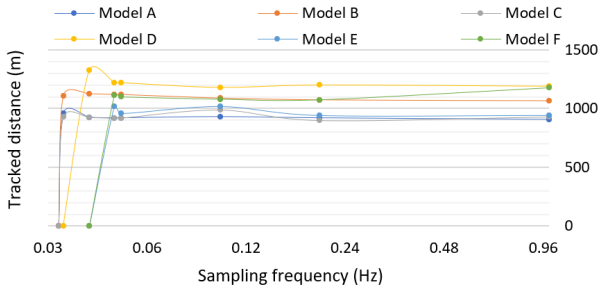

FIGURE 13. Result plotting the convergence study with six different plume models.

TABLE 4. The useable ranges of each coefficient for each angle term.

Factor	Recommended range
$Threshold_{ENTRE}$	$0.001 - 0.1$ % $Aggregate_{MAX}$
$Threshold_{MAX}$	$0.5 - 0.9$ % $Aggregate_{MAX}$
$Threshold_{MIN}$	$0.1 - 0.5$ % $Aggregate_{MAX}$
weighting-factor	$0.01 - 0.2$
offset	10 - 25°

near the strait in the South-East corner. This was because a lower weight allocated to the *edge angle* reduced the directional influence provided by the algorithm in detecting the position of the plume relative to the AUV and which enabled the vehicle to avoid the components of the plume and traverse the strait. Recommended ranges of each coefficient obtained through the sensitivity study are given in Table 4. A combined sensitivity study of AUV response caused by *weighting-factor* and *offset* is described in the discussion section.

C. MISSION OUTPUTS: PLUME MAP AND SAMPLES

In the process of tracking, the *mapping function* maps a part of the plume. The measured data from the sonar detection model, which is in the AUV local frame of reference, were transformed so that the sensed plume could be recorded on an empty map in the global frame of reference as shown in Figure 16.

Once the tracking and mapping were complete, the sampling mode (Mode 4) was successfully executed in all cases. The centroid was found within a margin of error of 1m and the virtual water sampler was triggered as marked by the blue cross.

IV. DISCUSSION

In the process of developing this adaptive sampling algorithm, we analysed the effects of each coefficient or parameter and how they affected the tracking performance of the algorithm. The results are presented here to assist future users in the practical use of the method.

We compared two *weighting-factor* cases (0.01 and 0.2) with five different *offset* values (10, 15, 20, 25 and 30). A *weighting-factor* of 0.01 means 1% (and 0.2 means 20%) of the *proximity angle* term, while the rest of the weight goes to the other angle terms in the decision-making process. Different trends were observed in terms of the tracked path (See Appendix). In general, a lower *weighting-factor* (0.01) led to more stable tracking over a wider range of *offset*, while a higher *weighting-factor* (0.2) produced a track trajectory at a greater distance from the plume. Also, a higher positive *weighting-factor* led to a greater repulsive reaction from the plume with increase of *offset* (see δ, ε, ζ and ν in the Appendix). This implies that *weighting-factor* had a more influential repulsive force with respect to the plume compared with *offset*. Another effect of setting a higher *offset* was that the AUV tracked outside of more of the small "islands" of low oil density that were around the plume (see $\beta - \zeta$, $\theta - \kappa$, $\iota - \xi$, $\lambda - \mu$ and $\gamma - \delta$ in the Appendix). The *proximity angle* term resulted in a linear repulsive displacement while the *adjustment angle* term was linked to an angular repulsive change to the AUV heading. Having both terms increased (see η in CASE-V in the Appendix), the vehicle lost track

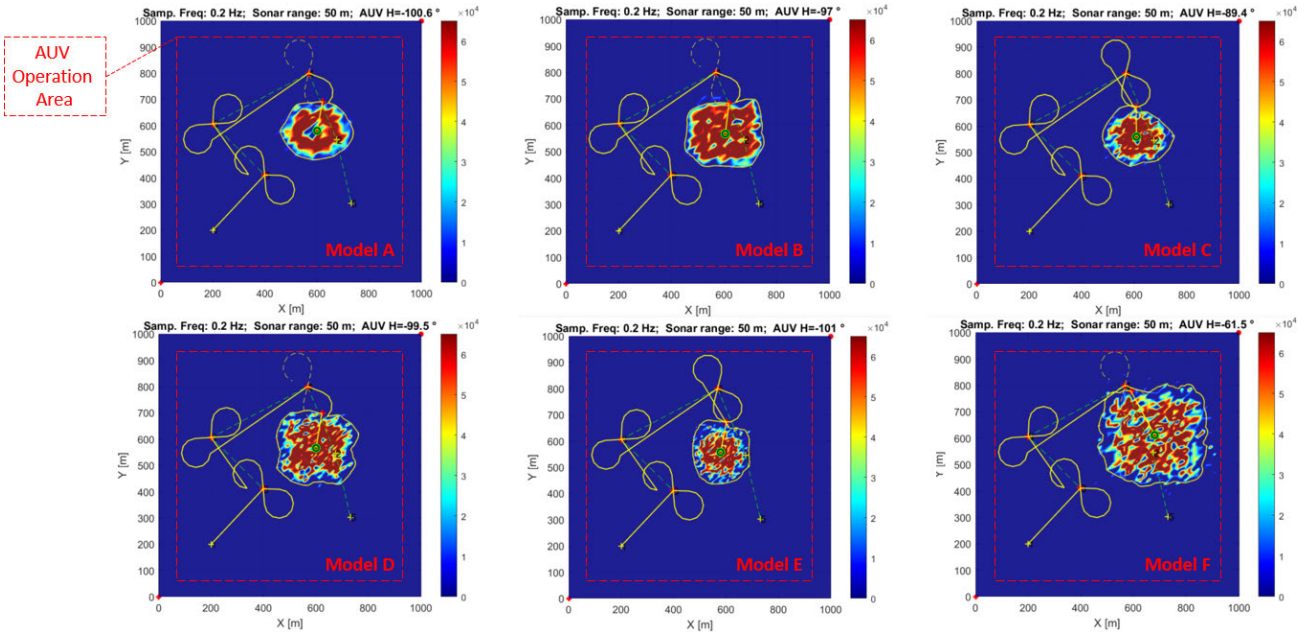

FIGURE 14. AUV trajectory tracking for different oil plume models A, B, C, D, E and F. The AUV operational area is marked by the dotted line.

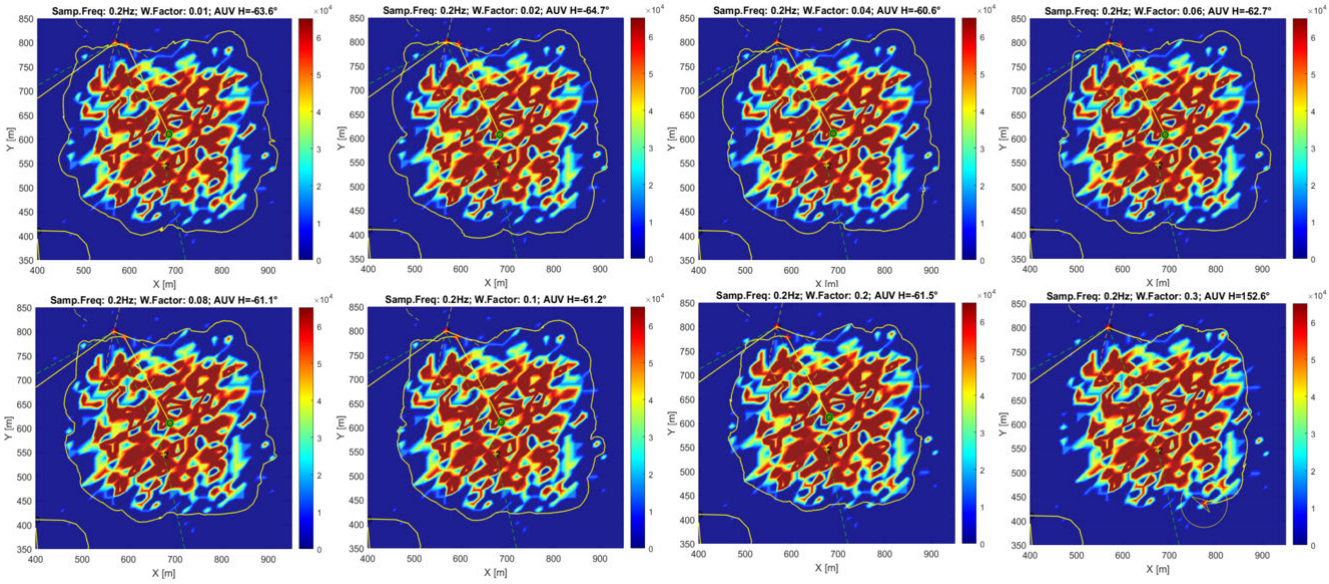

FIGURE 15. Simulated AUV trajectories during a sensitive study that varied the weighting-factor; 0.01, 0.02, 0.04, 0.06, 0.08, 0.1, 0.2 and 0.3.

of the plume. In contrast, the vehicle tracked the plume in the tightest manner when both terms were low (see α in CASE-VI in the Appendix).

The way in which *offset* and $p_{coefficient}$ influenced the AUV track differed. The $p_{coefficient}$ controls overall proximity to the plume based on the value of *Aggregate*, the sum of total detected area and oil plume density, with respect to the *thresholds* by forcing the AUV away from the plume if negative and towards the plume if positive (See Figure 17). On the other hand, the *offset* determined the heading angle for the AUV to take relative to the plume boundary and controlled the amount of the offset. In the presence of an oil patch, a low *offset* brought about a modified response to a sudden increase in the value of *Aggregate* by setting a heading angle closer to the plume. Hence, the *offset* reduced the ''flip-flop'' nature of the repelling reaction caused by the *proximity angle*.

The vertical dimension can also play an important role in detection. A level of 3D was taken into account through the vertical beam width of the sonar (25 degrees) which leads to an averaged response to the oil plume over a range of depth. In a true 3D survey, a strategy would be needed to track the plume depending on the 3D structure of the oil in the water

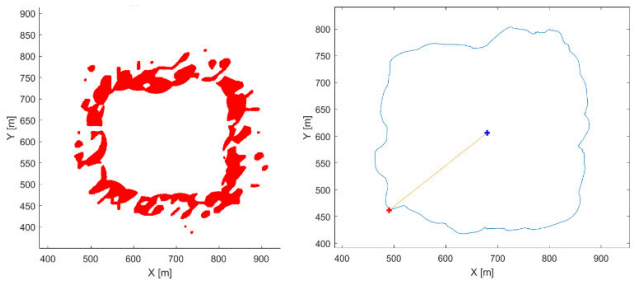

FIGURE 16. Boundary plot of the mapped plume (left); AUV trajectory during Mode 3: Tracking is shown by the blue line and Mode 4: Sampling is shown by the yellow line (right).

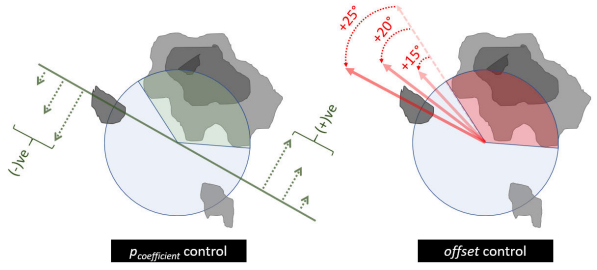

FIGURE 17. Comparison of the principles between $p_{coefficient}$ control and offset control.

column. For example, in calm water, with the oil on the water surface, the oil does not extend substantially over depth, but in a high energy wave environment, the waves can push the oil down into the water column, or if the oil on the surface is a result of oil released from a depth, then there may be pillars of oil rising from a depth in the water column. To be able to track such oil plumes, an appropriate sonar strategy is needed.

The sonar measurements were considered free of noise and other spurious data in our simulation. However, a real sonar system will have noise and false positive signals owing to substances other than oil in the water column. These need to be filtered in the in-situ analysis prior to using the output for autonomous decision making. In future field work we will collect realistic sonar data from an AUV. This will be used to refine the analysis to include signal filtering.

Our algorithm has advanced existing published plume tracking methods by allowing for discontinuous plumes and plumes made up of discrete elements, in this case oil droplets. Future work will involve developing the algorithm to model dynamic data which evolves over time in order to more accurately address a dispersing plume over a certain period of time and the time delays inherent in the collection of the scanning sonar data.

V. CONCLUSION AND FUTURE WORK

In this paper, we formulated a decision-making architecture for the problem of setting a path to track a discontinuous and realistic oil plume using an AUV. We have presented an adaptive algorithm tracking a virtually generated oil plume in a simulated environment. The plume characterized oil mixed in water consisting of a myriad of oil droplets forming a discontinuous plume with varied density.

The overall method was validated by using simulated sensor inputs and outputs. The AUV was instructed to manoeuvre itself around and map the plume and then to take a sample at the location that was in the centroid of the mapped plume. The results summarize the performance of the adaptive algorithm and characterize the influence of each component term in the decision-making process of the algorithm.

We successfully tracked a planar oil plume in a simulated environment by using an acoustic sensor model developed for in-situ analysis and by sending heading angle commands to the AUV vehicle control computer. The algorithm was found to work well in the sense that it could effectively respond to an irregularly shaped oil plume with patches, corners and complex boundaries. To date, the sensor model collected data in the two-dimensional plane, and hence it provided a two-dimensional map of the oil plume around the AUV. By accommodating an approach using a survey, the system overcomes the limitations involved with existing gradient-following methods. The approach demonstrates a robust and resilient algorithm and especially an approach that is able to deal with regions of multiple small oil patches, which require observations to be made beyond the edge of the target in order that a better decisions are made on the track of the vehicle.

Our oil plume tracking algorithm works by taking into account the multiple independent behaviours and objectives required by the vehicle: to keep a safe distance from the plume; to follow the plume edge; and to maintain progress around the plume. To fulfill these objectives, the sensitivity of the various parameters in the algorithm and their contribution to robustness must be considered. The set of threshold values (*Thresholds*) based on the summation quantities of sonar returns taken to be from oil in the water over a 360 degree scan around the AUV ($Aggregate_{MAX}$) were used to define when the AUV had encountered the plume; when it had lost contact with the plume; and minimum and maximum levels that needed to be maintained as the AUV tracked around the plume. These latter enabled a safe distance to be maintained between the AUV and the plume. Two other parameters, *weighting-factor* and *offset*, formed attraction and repulsion impacts on the tracking as well as created the impetus for the AUV to maintain progress around the plume. Tuning these two parameters was found to be key to successful plume delineation. The effective working range of the *weighting-factor*, through $p_{coefficient}$ control, was between 0.01 and 0.2; too high and the AUV tracked towards and then away from the plume in a flip-flop manner, however, did not progress around the plume. The working range of the *offset* control, the parameter which enabled the vehicle to progress around the plume, was between 15 and 25°. Although these are our recommendation ranges, a future user might tune the parameters to best suit an individual mission. For example, the parameters $Threshold_{ENTRE}$ and $p_{coefficient}$ need to be tuned so that the vehicle ignores small patches of oil and progresses past them; otherwise the AUV would respond

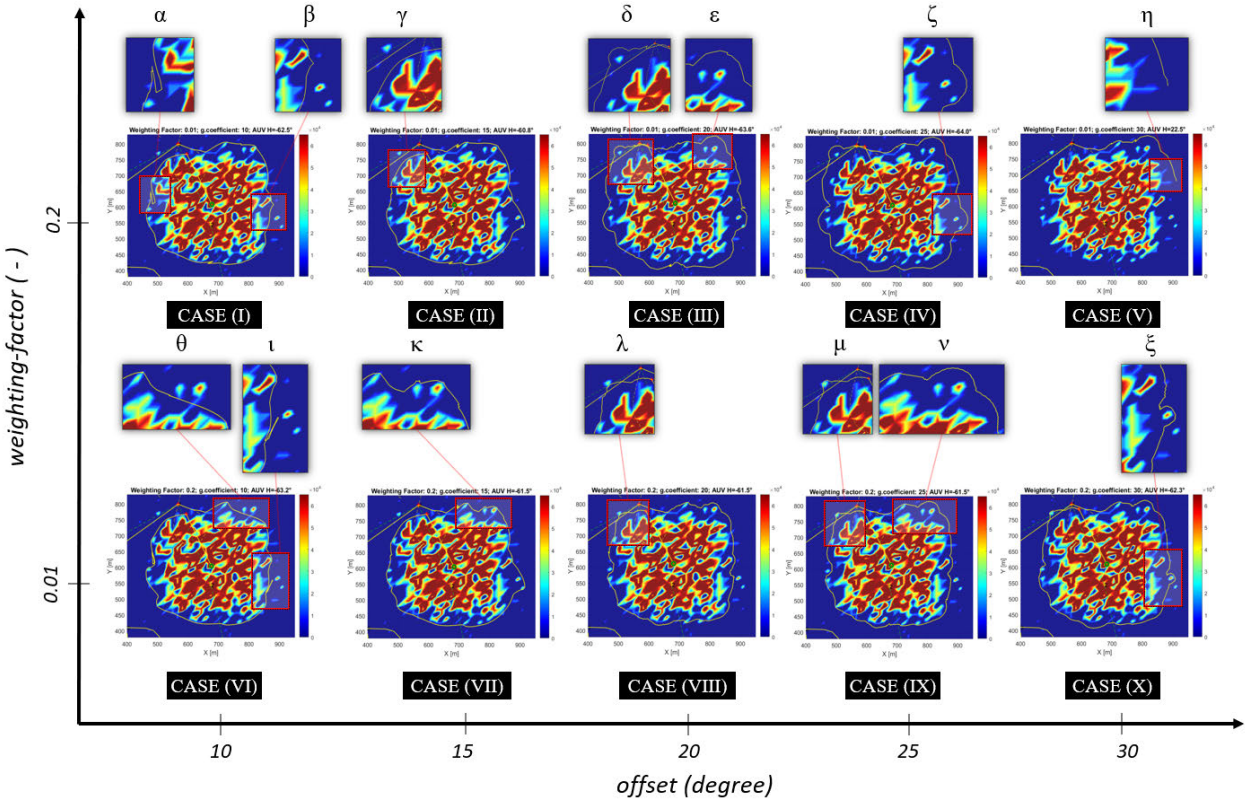

FIGURE 18. Sensitivity study showing trends in the AUV's plume tracking path from various combined parameters, *weighting-factor* (0.01 and 0.2) and *offset* (10, 15, 20, 25 and 30).

to and track every small patch of oil in the water column. On the other hand, if the *weighting-factor* is minimized and a low *offset* value is set for a mission, the AUV will follow every detail around the edge of the plume. To prevent the vehicle from getting stuck during tracking or losing contact with the plume, we had to adjust and tune the *thresholds* and *weighting-factor*.

The convergence study shows that updating the sonar data at a high sampling frequency is restricted by the speed of sonar scanning and the limited processing capability of the on-board computer. In addition, the in-situ sonar analysis model may be confounded by a number of other undesired manmade or natural sources of acoustic signals which can confuse our algorithm; such as fish, marine animals or ship propellers. For a robust, effective and efficient oil delineating application, acoustic sensing alone may not be sufficient. Nonetheless, in an environment where an oil plume is known to exist, sonar sensing can be useful and allows a potential oil plume to be sensed from a distance. To enhance decision autonomy on a sensor driven AUV, construction of adaptive algorithms suited for subsurface surveys are a basic essential.

The work has taken a step beyond existing plume mapping involving adaptive control based on gradient following methods. It has also developed a possible solution for practical problems and limitations of conventional approaches.

Potentially the approach is not limited to oil plumes, rather it might be applied for other underwater targets with similar discontinuous physical features such as tracking a school of fish, phytoplankton layers or locating black smokers on the seabed.

In future work, our aim is to take these results and advance the capability of the designed algorithm to address survey of three-dimensional regions and to tackle the spatial-temporal issues that result in tracking a dynamic (moving) plume that is commonly the case in reality owing to currents. Our aim is to equip our AUV with true intelligence.

APPENDIX

See Figure 18.

REFERENCES

[1] S. E. Chang, J. Stone, K. Demes, and M. Piscitelli, "Consequences of oil spills: A review and framework for informing planning," *Ecol. Soc.*, vol. 19, no. 2, pp. 1–25, 2014.

[2] R. N. Conmy, T. King, B. Robinson, S. Ryan, Y. Lu, M. Abercrombie, M. Boufadel, and H. Niu, "Dispersant effectiveness, *in-situ* droplet size distribution and numerical modeling to assess subsurface dispersant injection as a deepwater blowout oil spill response option and evaluation of oil fluorescence characteristics to improve forensic response tools," Environ. Protection Agency (EPA), Washington, DC, USA, Tech. Rep. EPA/600/R-16/152, 2016. [Online]. Available: https://www.epa.gov/research

[3] N. R. Council, *Oil in the Sea III: Inputs, Fates, and Effects*. Washington, DC, USA: National Academies Press, 2003.

[4] J. Hwang, N. Bose, S. Fan, B. Robinson, and K. Tenekedjiev, "Complications of robotic delineation of oil spills at sea," in *Proc. Int. Assoc. Maritime Universities (IAMU) Conf.*, 2019, pp. 26–33.

[5] J. W. Weaver, *Characteristics of Spilled Oils Fuels and Petroleum Products: 3a. Simulation of Oil Spills and Dispersants Under Conditions of Uncertainty*. Research Triangle Park, NC, USA: National Exposure Research Laboratory Office of Research and Development U.S. Environmental Protection Agency, 2004.
[6] J. A. Farrell, S. Pang, and W. Li, "Chemical plume tracing via an autonomous underwater vehicle," *IEEE J. Ocean. Eng.*, vol. 30, no. 2, pp. 428–442, Apr. 2005.
[7] J. Hwang, N. Bose, and S. Fan, "AUV adaptive sampling methods: A review," *Appl. Sci.*, vol. 9, no. 15, p. 3145, Aug. 2019.
[8] T. Lookman, P. V. Balachandran, D. Xue, and R. Yuan, "Active learning in materials science with emphasis on adaptive sampling using uncertainties for targeted design," *npj Comput. Mater.*, vol. 5, no. 1, pp. 1–17, Dec. 2019.
[9] H. Liu, Y.-S. Ong, and J. Cai, "A survey of adaptive sampling for global metamodeling in support of simulation-based complex engineering design," *Struct. Multidisciplinary Optim.*, vol. 57, no. 1, pp. 393–416, Jan. 2018.
[10] W. Huang, T. Zhang, Y. Rong, and J. Huang, "Adaptive sampling towards fast graph representation learning," in *Proc. Adv. Neural Inf. Process. Syst.*, 2018, pp. 4558–4567.
[11] J. Hwang, N. Bose, H. D. Nguyen, and G. Williams, "Acoustic search and detection of oil plumes using an autonomous underwater vehicle," *J. Mar. Sci. Eng.*, vol. 8, no. 8, p. 618, Aug. 2020.
[12] Z. Kashino, G. Nejat, and B. Benhabib, "A multi-robot sensor-delivery planning strategy for static-sensor networks," in *Proc. IEEE/RSJ Int. Conf. Intell. Robots Syst. (IROS)*, Sep. 2017, pp. 6640–6647.
[13] R. Cristi, M. Caccia, G. Veruggio, and A. J. Healey, "A sonar based approach to AUV localization," *IFAC Proc. Volumes*, vol. 28, no. 2, pp. 291–298, May 1995.
[14] K. R. Reisenbichler, M. R. Chaffey, F. Cazenave, R. S. McEwen, R. G. Henthorn, R. E. Sherlock, and B. H. Robison, "Automating MBARI's midwater time-series video surveys: The transition from ROV to AUV," in *Proc. OCEANS MTS/IEEE Monterey*, Sep. 2016, pp. 1–9.
[15] J. P. Wilkinson, T. Boyd, B. Hagen, T. Maksym, S. Pegau, C. Roman, H. Singh, and L. Zabilansky, "Detection and quantification of oil under sea ice: The view from below," *Cold Regions Sci. Technol.*, vol. 109, pp. 9–17, Jan. 2015.
[16] K. Kim, N. Neretti, and N. Intrator, "Mosaicing of acoustic camera images," *IEE Proc.-Radar, Sonar Navigat.*, vol. 152, no. 4, pp. 263–270, 2005.
[17] M. F. Fallon, M. Kaess, H. Johannsson, and J. J. Leonard, "Efficient AUV navigation fusing acoustic ranging and side-scan sonar," in *Proc. IEEE Int. Conf. Robot. Automat.*, May 2011, pp. 2398–2405.
[18] S. Barkby, S. Williams, O. Pizarro, and M. Jakuba, "An efficient approach to bathymetric SLAM," in *Proc. IEEE/RSJ Int. Conf. Intell. Robots Syst.*, Oct. 2009, pp. 219–224.
[19] K. Teo, K. W. Ong, and H. C. Lai, "Obstacle detection, avoidance and anti collision for MEREDITH AUV," in *Proc. OCEANS*, Oct. 2009, pp. 1–10.
[20] J. Hwang, S. Fan, P. King, and A. Forrest, "Development of error reduction model using Bayesian filter for AUV navigating under moving ice," in *Proc. IEEE/OES Auton. Underwater Vehicle Workshop (AUV)*, Nov. 2018, pp. 1–6.
[21] B. Zhang and G. S. Sukhatme, "Adaptive sampling for estimating a scalar field using a robotic boat and a sensor network," in *Proc. IEEE Int. Conf. Robot. Automat.*, Apr. 2007, pp. 3673–3680.

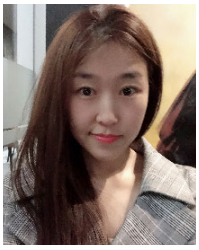

JIMIN HWANG received the B.E. degree (Hons.) in naval architecture from the Australian Maritime College (AMC), University of Tasmania, Launceston, TAS, Australia, in 2016. She is currently pursuing the Ph.D. degree in maritime engineering with AMC. Her thesis work focused on localization of autonomous underwater vehicles (AUVs) in a moving frame of reference.

Her project involves algorithm development of in-situ data-driven adaptive systems to control an AUV for tracking an oil plume. Her research interests include application of underwater robots for marine environmental problems, development of sensor-based reacting systems, and the design of artificial intelligence autonomous-decision making systems for marine robots.

Ms. Hwang was a recipient of the Tasmanian International Scholarship, Australian Government Research Training Program Scholarship and Antarctic Gateway Partnership Scholarship.

NEIL BOSE received the B.Sc. degree in naval architecture and ocean engineering and the Ph.D. degree from the University of Glasgow, in 1978 and 1982, respectively.

He was an Assistant Professor with the Naval Architectural Engineering Program, Memorial, in May 1987. He joined the Australian Maritime Hydrodynamics Research Centre, Australian Maritime College (AMC), as the Manager, in 2007. He was also a Professor of maritime hydrodynamics with AMC. From 2009 to 2011, he was the Director of the AMC's National Centre for Maritime Engineering and Hydrodynamics. From 2012 to 2017, he was a Principal with AMC, University of Tasmania. He was appointed as the Vice-President (Research) with the Memorial University of Newfoundland, Canada, in 2017. His research interests include marine propulsion, autonomous underwater vehicles, ocean environmental monitoring, ocean renewable energy, ice/propeller interaction, and aspects of offshore design.

HUNG DUC NGUYEN (Member, IEEE) was born in Haiphong, Vietnam. He received the Bachelor of Engineering degree in ship navigation from Vietnam Maritime University, and the Master of Engineering degree in marine systems engineering and the Ph.D. degree in marine control engineering from the Tokyo University of Marine Sciences and Technology, in 1998 and 2001, respectively.

From April 2001 to August 2002, he worked with Japanese Nuclear Instrumentation Company, Japan. Since September 2002, he has been a Lecturer in maritime engineering with the Australian Maritime College, University of Tasmania, Launceston, TAS, Australia. His research interests include modeling and system identification of dynamic systems, self-tuning, optimal and intelligent control, guidance, navigation and control of marine vehicles including autonomous surface, underwater and remotely operated vehicles, and marine electrical electronic systems.

Dr. Nguyen has memberships of the Institute of Navigation (ION), USA, and the Japan Institute of Navigation (JIN), Japan. He received several award/s, including The Royal Institution of Naval Architects Medal of Distinction for a coauthored paper, in 2017.

GUY WILLIAMS received the Bachelor of Aeronautical Engineering degree from The University of Sydney, in 1995, developing an interest in fluid dynamics and control systems, and the Ph.D. degree in antarctic physical oceanography led to an Arctic Research Voyage, in 2004, where he observed the ground-breaking deployments of the UK's Autosub-II AUV.

He has been a Polar Oceanographer, specializing in the use of autonomous platforms (including instrumented seals) to study the cryosphere. From 2012 to 2017, he led the deployment of AUVs and drones from Australian and US icebreakers to study Antarctic and Arctic sea-ice from above and below, through an ARC Future Fellowship, from 2013 to 2018. He was the Science Coordinator for the Antarctic Gateway Partnership's Explorer-class AUV Program, in 2018, where he is currently the AMSL Lead. He is excited by the massive potential for autonomous platforms to survey challenging oceanic environments, filling data gaps that guarantee paradigm shifts in our understanding of the planet and ability to predict its future.